

www.acsaem.org Article

Machine Learning Assisted Analysis of Electrochemical H₂O₂ Production

Juyoung Leem, Lauren Vallez, Thomas Mark Gill, and Xiaolin Zheng*



Cite This: ACS Appl. Energy Mater. 2023, 6, 3953–3959



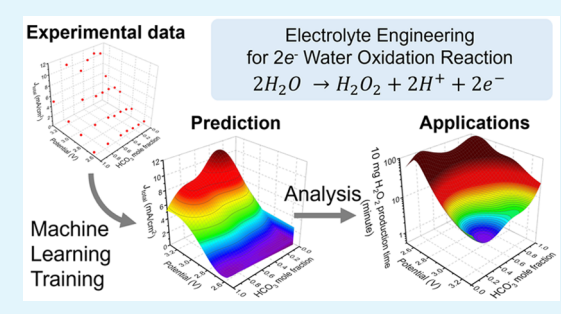
ACCESS I

III Metrics & More

Article Recommendations

Supporting Information

ABSTRACT: The two-electron water oxidation reaction ($2e^-$ WOR) provides an option for on-site production of the valuable chemical hydrogen peroxide (H_2O_2). A major challenge for the $2e^-$ WOR is the need to improve its selectivity toward H_2O_2 over O_2 production through the oxygen evolution reaction. Electrolyte engineering has shown great promise in improving the selectivity and production rates toward H_2O_2 . However, experimental efforts in optimizing the electrolyte only yield results at discrete conditions, which does not provide a complete picture of performance over the entire parameter range. Here, we apply a machine learning assisted prediction to map out the performance of electrochemical H_2O_2 production over the continuous parameter space of electrolyte composition and applied potential.



We collected experimental data of faradaic efficiencies ($FE_{\rm H_2O_2}$) and current densities toward $\rm H_2O_2$ ($J_{\rm H_2O_2}$) as functions of the applied potential and carbonate ion mole fractions ($\rm HCO_3^-$ and $\rm CO_3^{2-}$) in the electrolyte. The data were then used to train a support vector regression model with 5-fold cross-validation. The accuracy of the model was verified against additional experimental results. The model identified that a maximum $\rm H_2O_2$ current density of 2.16 mA/cm² can be achieved from an optimized bicarbonate ion mole fraction of 0.225 at an applied potential of 3.25 V vs RHE. Lastly, the continuous model enables us to evaluate the thermal efficiency, $\rm H_2O_2$ electricity cost, and time needed to produce a set amount of $\rm H_2O_2$ over a broad range of electrolytes and applied potential conditions. This work demonstrates how machine learning enables the use of discrete experimental points to construct a continuous picture of electrochemical $\rm H_2O_2$ production with high accuracy.

KEYWORDS: electrolyte engineering, two-electron water oxidation, machine learning, sustainable chemical production, electrochemical hydrogen peroxide production, H_2O_2

■ INTRODUCTION

Hydrogen peroxide (H_2O_2) has been widely used for disinfection, chemical processing, water treatment, and bleaching, in industry, research laboratories, hospitals, and households. Recently, distributed electrochemical production of H_2O_2 , in place of the centralized anthraquinone process, has attracted growing attention as a candidate for sustainable chemical processes and energy storage. Electrochemical production of H_2O_2 through the two-electron water oxidation reaction $(2e^-WOR)^{9,12}$ only requires water as the reactant to produce H_2O_2 . However, $2e^-WOR$ competes with a thermodynamically more favorable reaction—the oxygen evolution reaction (OER). Thus, improving selectivity toward the $2e^-WOR$ has been one of the major challenges in the electrochemical production of H_2O_2 .

The performance of the $2e^-$ WOR is influenced by various factors including the catalyst material, electrolyte ions, applied potential, and temperature. Among those, the effect of the electrolyte had not been thoroughly investigated until recently. An electrolyte composed of bicarbonate (HCO_3^-) ions is known to promote H_2O_2 production in electrochemical systems, and it has been reported that tuning carbonate

ionic species (i.e., HCO_3^- and CO_3^{2-}) can improve selectivity toward H_2O_2 production by 9-fold. ^{16,17} Electrolyte engineering for the $2e^-$ WOR has shown exciting promise, yet the theoretical foundation and mechanism behind the effect of carbonaceous electrolytes for H_2O_2 production have not been fully understood. ¹⁶ Thus, the effect of the electrolyte on the $2e^-$ WOR is not easily predicted through traditional approaches, such as the computational or physical/chemical model-based approach. Instead, a data-driven approach, which utilizes data to investigate a system, is unexplored and yet suitable to study and optimize the electrolyte for $2e^-$ WOR. ¹⁸

In this work, we demonstrate how machine learning enables the use of discrete experimental points to construct a continuous picture of the effect of the applied potential and electrolyte mole fraction on the electrochemical production of

Received: January 17, 2023 Accepted: March 22, 2023 Published: March 30, 2023





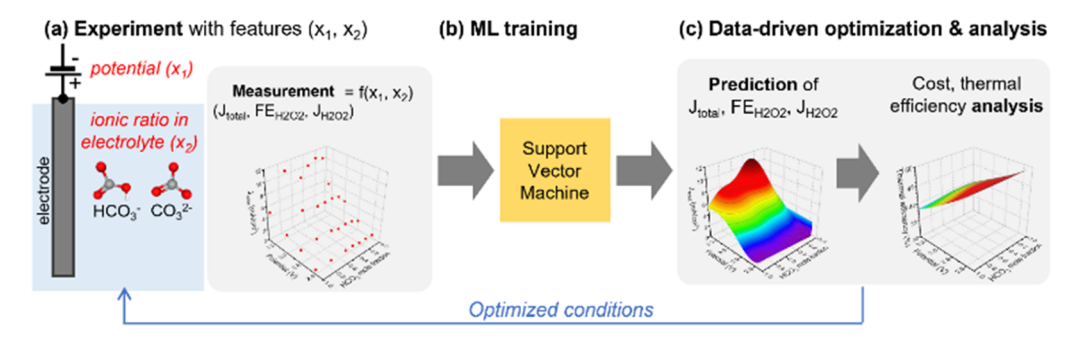


Figure 1. Data-driven optimization and analysis process for electrochemical production of H_2O_2 via $2e^-$ WOR. (a) Total current density (J_{total}), faradaic efficiency ($FE_{H_2O_2}$), and current density toward H_2O_2 production ($J_{H_2O_2}$) were collected from $2e^-$ WOR with different potential and carbonate ionic ratios in the electrolyte. (b) We trained a support vector regression (SVR) model to predict J_{total} , $FE_{H_2O_2}$, and $J_{H_2O_2}$ in the given potential— HCO_3^- fraction (x_1-x_2) space. (c) Data-driven predictions provide us with continuous maps showing J_{total} , $FE_{H_2O_2}$, and $J_{H_2O_2}$ changes and trends in the feature space. The prediction results were also used for cost, production time, and efficiency analyses for further applications.

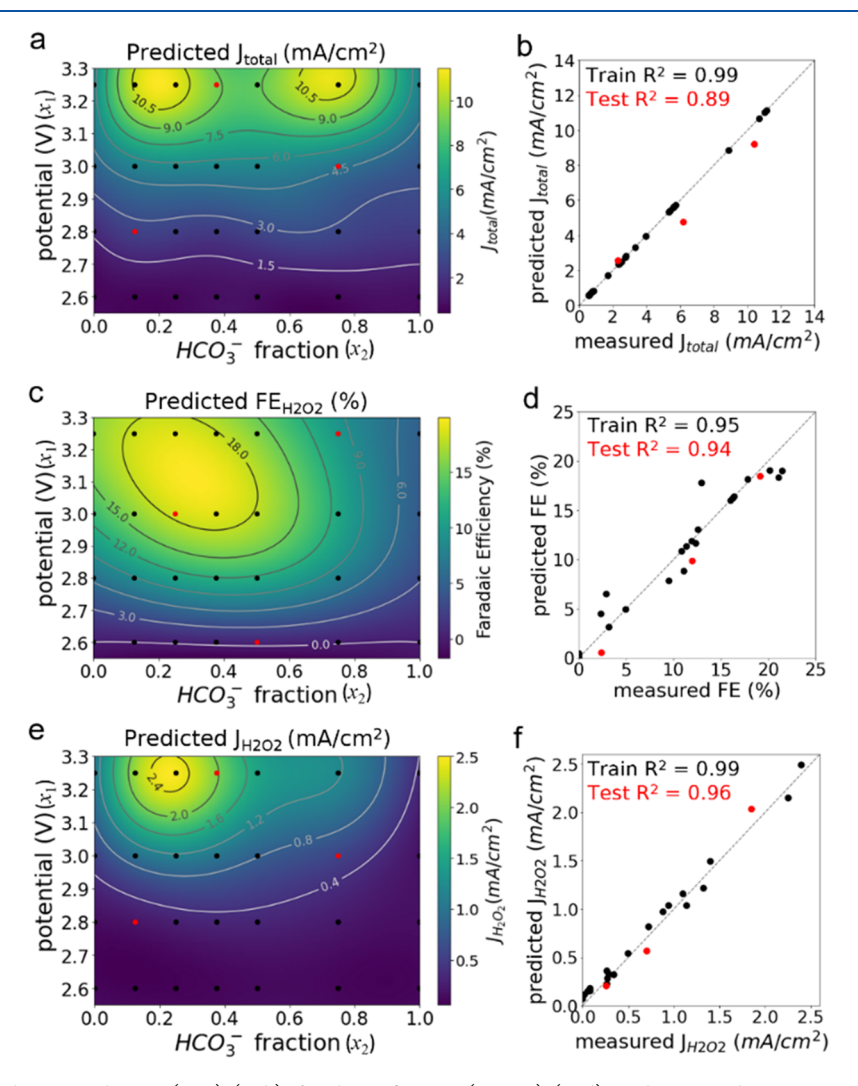


Figure 2. Prediction of total current density (J_{total}) (a, b), faradaic efficiency $(FE_{\text{H}_2\text{O}_2})$ (c, d), and current density toward H_2O_2 production $(J_{\text{H}_2\text{O}_2})$ (e, f). In contour plots and scattered plots, black scatters indicate data points assigned in the training sets, and red scatters indicate data points assigned in the test sets.

 ${
m H_2O_2}$ via the $2{
m e^-}$ WOR with high accuracy. To demonstrate the new approach, we chose two independent parameters of the electrochemical system. First, the total current density $(J_{\rm total})$, faradaic efficiency $(FE_{{
m H_2O_2}})$, and current density toward ${
m H_2O_2}$ production $(J_{{
m H_2O_2}})$ were collected experimentally at

various applied potentials and electrolyte ion mole fractions. We then used the data to train a support vector regression (SVR) model 19 with radial basis function (rbf) as the kernel function. The trained model accurately predicts the values of J_{total} , $FE_{\text{H}_2\text{O}_2}$, and $J_{\text{H}_2\text{O}_2}$ at applied potentials and electrolyte ion

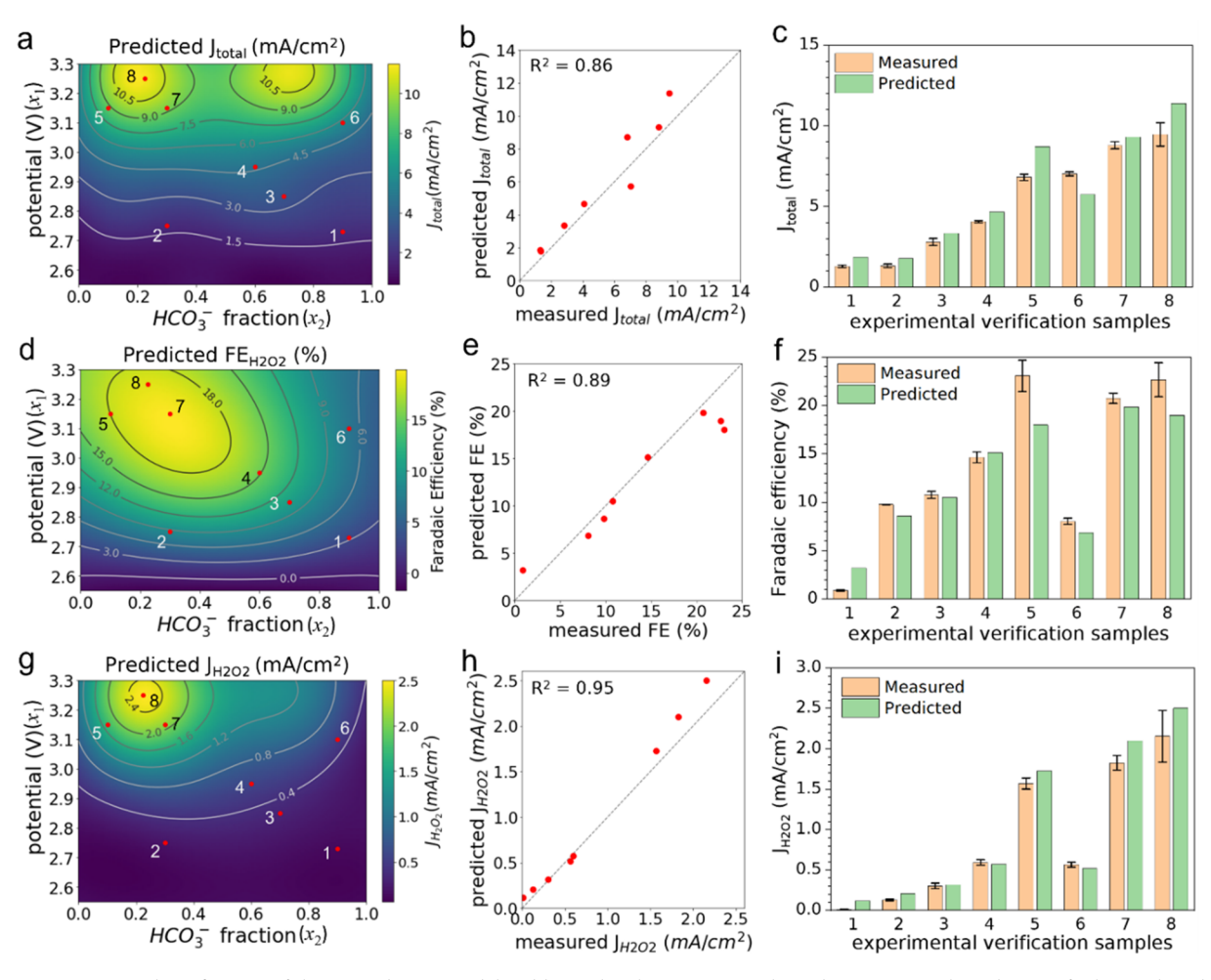


Figure 3. Experimental verification of the trained SVR model. Additional eight experimental conditions were selected to verify the predicted values of J_{total} (a-c), $FE_{\text{H}_2\text{O}_2}$ (d-f), and $J_{\text{H}_2\text{O}_2}$ (g-i). Trained models successfully predicted the experimental verification data points with high R^2 scores of 0.86 for J_{total} , 0.89 for $FE_{\text{H}_2\text{O}_2}$, and 0.95 for $J_{\text{H}_2\text{O}_2}$ prediction. In panels c, f, and i, error bars indicate 1 standard deviation on average of three measurements.

mole fractions domains that were not measured previously, which we verified by newly obtained experimental data. The experimental verification results clearly show that our ML assisted process can predict results of unseen experimental conditions, provide a complete picture of the current densities and faradaic efficiencies in the parameter space, and confirm the optimum conditions to maximize $FE_{\rm H_2O_2}$ or $J_{\rm H_2O_2}$. Lastly, we demonstrate that the model enables us to evaluate the electrolyte impact on thermal efficiency, electricity cost for $\rm H_2O_2$ production, and $\rm H_2O_2$ production time.

RESULTS AND DISCUSSION

Figure 1 illustrates our overall ML assisted process for electrochemical $\rm H_2O_2$ production, which involves experimental data collection, ML model training, and optimization and analysis steps. For electrochemical $\rm H_2O_2$ production, we focus on anodic production through the $\rm 2e^-$ WOR. $\rm ^{13,20}$ Our independent input parameters are the applied potential (x_1) and electrolyte composition in terms of the $\rm HCO_3^-$ mole fraction (x_2) as shown in Figure 1a. Our output parameters of interest are $J_{\rm total}$, $FE_{\rm H_2O_2}$, and $J_{\rm H_2O_2}$ (Figure 1a). Next, we used the data to train an SVR model with x_1 and x_2 as features (Figure 1b). The trained SVR model predicts changes in $J_{\rm total}$)

 $FE_{\rm H_2O_2}$, and $J_{\rm H_2O_2}$ in two-dimensional feature space (x_1 – x_2 ; potential and HCO $_3$ ⁻ mole fraction) (Figure 1c). We then went back and experimentally confirmed random results predicted by the model. Finally, because these predicted contours are continuous functions of x_1 and x_2 , we use them to estimate thermal efficiency, H_2O_2 electricity cost, and H_2O_2 production time in the two-dimensional feature space. The prediction and analysis results can be used in finding the optimized conditions for the greatest H_2O_2 production rate, highest thermal or faradaic efficiency, lowest H_2O_2 electricity cost, or fastest H_2O_2 production.

We experimentally measured J_{total} , $FE_{\text{H}_2\text{O}_2}$, and $J_{\text{H}_2\text{O}_2}$ at 28 conditions in the potential range from 2.6 to 3.25 V and the HCO_3^- mole fraction range from 0 to 1 (where a HCO_3^- mole fraction of 0 is an electrolyte of pure K_2CO_3 and a HCO_3^- mole fraction of 1 is an electrolyte of pure KHCO_3). To utilize those data for our subsequent SVR training, we define the applied potential in V vs RHE as x_1 and the mole fraction HCO_3^- in the electrolyte mixture of KHCO_3 and K_2CO_3 as x_2 . We used the 28 data points with features of x_1 and x_2 to train an SVR model and evaluate the trained model (Table S1). We used the coefficient of determination (R^2) as the model evaluation metric, and a perfectly accurate prediction would

yield an R² value of 1. We tried different data set splitting strategies and chose the best model to maximize the R^2 values (Figures S4 and S5). As shown in Figure 2, the experimental data are scattered yielding discrete points of J_{total} , $FE_{\text{H-O-}}$, and J_{H₂O₂} (black dots for training data points and red dots for test data points), while the trained SVR model yields continuous values and trends of J_{total} , $FE_{\text{H}_2\text{O}_2}$, and $J_{\text{H}_2\text{O}_2}$ in the given feature space (color contours). Figure 2a shows that the total current density Jtotal generally increases with increasing applied potential (x_1) and shows little dependence on the HCO₃⁻ mole fraction (x_2) . Only when the applied potential reaches above 3.1 V, J_{total} is slightly affected by the HCO₃⁻ mole fraction, which could be attributed to experimental errors or more likely changes in the surface chemistry at the electrode/ electrolyte interface. ^{16,21–23} Figure 2b shows that the predicted Jtotal values are close to their measured values (Figure 2b) with high R^2 scores (train $R^2 = 0.99$; test $R^2 = 0.89$).

Figures 2c and 2e show that both $FE_{H_2O_2}$ and $J_{H_2O_2}$ depend strongly on the applied potential (x_1) and HCO_3^- mole fraction (x_2) . $FE_{H,O}$, and $J_{H,O}$ can vary vastly with the $HCO_3^$ mole fraction at a fixed applied potential and relatively consistent J_{total} values. For example, at an applied potential of 3.25 V, the predicted $J_{H_2O_2}$ values varied from 0.4 to over 2.4 ${\rm mA/cm^2},$ which supports the importance of optimizing electrolyte mole fraction for the $2{\rm e^-}$ WOR. 16,17 Moreover, the maximum $FE_{H_2O_2}$ peak occurs around the applied potential of 3.15 V and a HCO₃⁻ mole fraction of 0.3, which is different from the maximum $J_{H_2O_2}$ conditions (3.25 V, 0.232 HCO₃⁻ mole fraction). This difference in optimized conditions does not come as a surprise considering $J_{H_2O_2}$ is a function not only of the $FE_{H_2O_2}$ but also of J_{total} (refer to eq 5 in the Experimental Methods section). Specifically, $FE_{H_2O_2}$ often reaches a maximum at an applied potential $<3.25 \text{ V},^{12,24-26} \text{ while } J_{\text{total}}$ continues to increase with an increasing applied potential. Thus, the maximum $J_{\mathrm{H}_2\mathrm{O}_2}$ may not occur at the same condition as the highest FE_{H,O_2} . The maximum values of predicted J_{total} $FE_{H_2O_2}$, and $J_{H_2O_2}$ and their experimental conditions are presented in Table S3.

After training an SVR model, we demonstrate that the model can predict the experimental conditions necessary to achieve a desired current density or faradaic efficiency. We selected eight additional combinations of applied potentials and HCO_3^- mole fractions. The eight points are marked as red dots and labeled from 1 to 8 on the contour plots of J_{total} , $FE_{\text{H}_2\text{O}_2}$, and $J_{\text{H}_2\text{O}_2}$ in Figures 3a, 3d, and 3g, respectively. The additional points include untested points distributed in the feature space (#1–6), the highest predicted $FE_{\text{H}_2\text{O}_2}$ point (#7), and the highest predicted $J_{\text{H}_2\text{O}_2}$ point (#8). The values and conditions of eight data points used in the experimental verification are presented in Table S2. Figure 3 shows that the measured values of J_{total} , $FE_{\text{H}_2\text{O}_2}$, and $J_{\text{H}_2\text{O}_2}$ of those eight points agree well with the predicted ones. These results demonstrate the great potential of our approach for inverse-design applications.

As the model provides the prediction values of J_{total} , $FE_{\text{H}_2\text{O}_2}$, and $J_{\text{H}_2\text{O}_2}$ over the entire applied potential and HCO_3^- mole fraction parameter space, we can further evaluate the impact of those two parameters on the thermal efficiency of the system,

electricity cost of H_2O_2 production, and time needed to achieve a desired quantity of H_2O_2 (e.g., 10 mg), as shown in Figure 4.

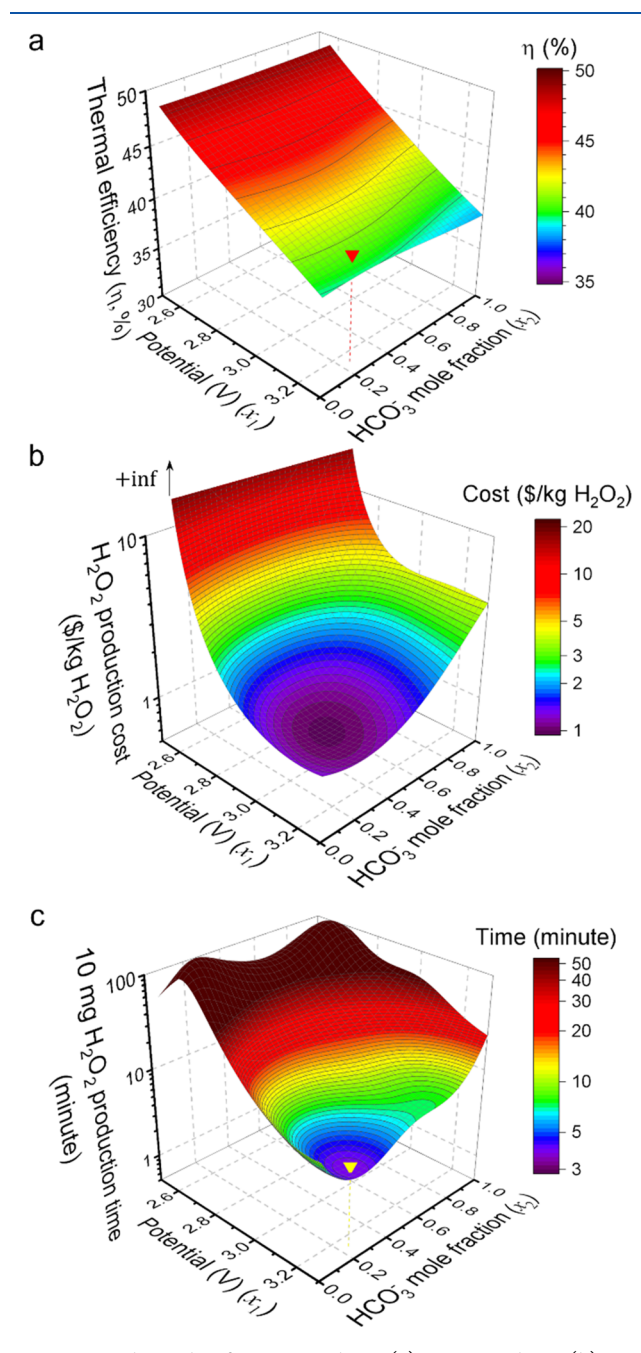


Figure 4. Thermal efficiency analysis (a), cost analysis (b), and production time estimation (c) of our system, based on predictions. (a) A red arrow points to our highest $J_{\text{H}_2\text{O}_2}$ condition ($\eta = 40.2\%$). The electricity cost of H_2O_2 production (b) diverges at a lower potential range as $FE_{\text{H}_2\text{O}_2}$ approaches zero. (c) A yellow arrow points at our shortest H_2O_2 production time (t = 3.8 min).

First, for the thermal efficiency calculation, we used lower heating values (LHV) to estimate the amount of energy stored in $\rm H_2O_2$ and $\rm H_2$ per mole and assumed that $\rm H_2$ production at the cathode yields 100% efficiency (see the Supporting Information for details). Thermal efficiency shows a strong dependence on the applied potential and weak dependence on

the electrolyte composition. Higher thermal efficiency of over 45% can be achieved in the lower potential range (<2.8 V). At our highest $J_{\text{H}_2\text{O}_2}$ condition, the thermal efficiency is 40.2% (red triangular mark in Figure 4a).

Second, Figure 4b shows the predicted electricity cost for producing 1 kg of $\rm H_2O_2$ by assuming that the electricity price is \sim \$40/MWh from renewable energy sources (see the Supporting Information for details). The $\rm H_2O_2$ production electricity cost is approximately inversely proportional to $\rm \it FE_{\rm H_2O_2}$. The minimum electricity cost of <\$1 per kg of $\rm H_2O_2$ occurs when the applied potential is between 3.0 and 3.1 V and the $\rm HCO_3^-$ mole fraction between 0.25 and 0.4. 27,28

Finally, Figure 4c shows the predicted time needed to produce 10 mg of $\rm H_2O_2$ assuming a 100 cm² anode (see the Supporting Information for details). The shortest time needed is only 3.8 min, which occurred at 3.25 V and a $\rm HCO_3^-$ mole fraction of 0.23 (yellow triangular mark in Figure 4c). While, unsurprisingly, much longer production times are needed at lower applied potentials. The cost and time needed for $\rm H_2O_2$ production are important parameters for the future implementation of the technology. Which parameter is valued most will depend on the application and will determine the conditions applied to the system. By using the predictions from the model as inputs, the efficiency, cost, and production time can be easily determined from these complete, continuous contour plots without the need for additional experiments.

The findings of our study demonstrate the effectiveness of incorporating machine learning in the field of experimentbased electrolyte engineering for H₂O₂ production. By utilizing discrete experimental data, the machine learning assisted approach allowed for the construction of continuous performance functions across the entire range of parameters examined. These functions can then be leveraged to optimize electrolyte conditions and to conduct further analysis of the electrochemical system. However, it is important to acknowledge that there are limitations to this approach. One significant constraint is the need for a large data set to train the machine learning models, which may require significant and sometimes unfeasible experimental effort. For instance, we conducted more than 100 experiments in this study to gather sufficient data to train and verify our models. To facilitate the application of machine learning assisted approaches in experimental studies, standardized experimental protocols and collaborative efforts to establish a database of experimental data will be crucial.

CONCLUSIONS

In conclusion, we have successfully demonstrated the efficacy of using machine learning to accelerate the optimization processes and to predict various performance parameters of electrochemical H_2O_2 production through the $2e^-$ WOR. We used 28 discrete experimental data points to train an SVR model that produces maps of J_{total} , $FE_{H_2O_2}$, and $J_{H_2O_2}$ in our feature space (x_1-x_2) with high accuracy. This two-dimensional continuous information onfers us a continuous picture of the current density and efficiency trends, which predict optimized conditions and provide some insights into the effect of the electrolyte on the $2e^-$ WOR. The machine learning prediction also enables us to evaluate the system, including thermal efficiency, electricity cost of the H_2O_2 production, and H_2O_2 production time, which can improve the design of these systems for practical applications. We believe such machine

learning assisted analyses will become a powerful tool in providing complete pictures and means of evaluating systems using discrete experimental data, especially for more complex systems with a higher-dimensional feature space with multiple factors.

EXPERIMENTAL METHODS

Electrochemical Data Collection. We prepared 1.7 cm \times 5 cm fluorine-doped tin oxide coated glass (FTO, 7–8 ohm/sq, TEC 7, MSE Supplies LLC) for the working electrodes. The samples were sonicated in acetone, isopropyl alcohol, and then deionized (DI) water before being rinsed with DI water and dried. Copper tape was attached to the FTO, and a silver paste was painted over the connection. Teflon tape was wrapped tightly around the electrical contact. The geometric area of the exposed FTO was measured using ImageI software and was used to normalize the current densities.

All electrolytes were prepared with a total dissolved inorganic carbon concentration of 1.5 M. The following equations were used to calculate the individual concentrations of KHCO₃ and K_2CO_3 depending on the desired HCO₃⁻ mole fraction:

$$X_{HCO_3} \times 1.5 \text{ M} = [KHCO_3] \tag{1}$$

$$(1 - X_{HCO_3}) \times 1.5 \text{ M} = [K_2CO_3]$$
 (2)

where $X_{\rm HCO_3}$ is the ${\rm HCO_3}^-$ mole fraction and [KHCO_3] and [K₂CO₃] are the molar concentrations in mol/L of KHCO₃ and K₂CO₃, respectively. After the correct amounts of KHCO₃ and K₂CO₃ were added to DI water, the solution was shaken and sonicated in an ice bath. The pH of the electrolyte was measured using a pH meter (Mettler-Toledo FP20) to convert the desired potential versus the reversible hydrogen electrode (vs RHE) to the experimental, applied potential versus the reference electrode (vs Ag/AgCl) via the following equation:

$$E_{Ag/AgCl} = E_{RHE} - (0.059 \times pH) - 0.199 V$$
 (3)

where 0.199 V is the potential of the Ag/AgCl reference electrode vs RHE provided by the manufacturer (Gamry Instruments). $E_{Ag/AgCl}$ is expressed in V vs Ag/AgCl, and $E_{\rm RHE}$ is expressed in V vs $m \ddot{R}H\ddot{E}$. A three-electrode configuration was used with FTO-coated glass as the working electrode, carbon paper as the counter electrode (Fuel Cell Store), and Ag/AgCl as the reference electrode. A potential ($E_{Ag/AgCl}$) was applied to the working electrode, and the current was measured using a potentiostat (Gamry Interface 1000). All results were collected in an electrochemical H-cell (Pine Research) immersed in an ice bath. Both chambers of the electrochemical H-cell were filled with the same electrolyte. The electrolyte in the anodic chamber was stirred using a magnetic stir bar to prevent a H₂O₂ concentration gradient. The uncompensated resistance was measured using a single point, high-frequency impedance measurement, which was then used to apply a positive-feedback iR compensation during the chronoamperometric tests. After a chronoamperometric test of 10 min, an aliquot was taken from the anodic chamber of the H-cell, and the amount of H₂O₂ was quantified using UV-visible (UV-vis) spectrophotometry (Agilent Cary 6000i) via the cobalt-carbonate assay²⁰ with an absorption feature at 260 nm. The calibration line used to convert UV-vis absorption to the amount of produced H₂O₂ is available in Figure S1. The $FE_{H_2O_2}$ and $J_{H_2O_2}$ were calculated using the following equations:

$$FE_{\rm H_2O_2} = \frac{[\rm H_2O_2] \times V \times 2 \times 96485 \frac{C}{\rm mol}}{q \times 34 \frac{g}{\rm mol}} \times 100 \tag{4}$$

where $FE_{\mathrm{H_2O_2}}$ is the faradaic efficiency toward $\mathrm{H_2O_2}$ expressed as a percentage, $[\mathrm{H_2O_2}]$ is the measured concentration of $\mathrm{H_2O_2}$ in g/mL, V is the electrolyte volume in mL, 2 is the stoichiometric number of electrons transferred for $\mathrm{H_2O_2}$ production via water oxidation, and q is the charge passed in coulombs.

$$J_{\rm H_2O_2} = J_{\rm total} \times \frac{FE_{\rm H_2O_2}}{100}$$
 (5)

where $J_{\text{H}_2\text{O}_2}$ is the current density toward H_2O_2 in mA/cm², J_{total} is the total current density in mA/cm², and $FE_{\text{H}_2\text{O}_2}$ is the faradaic efficiency toward H_2O_2 expressed as a percentage.

Machine Learning Training. We used support vector regression $(SVR)^{19}$ with radial basis function (rbf) as a kernel function to predict J_{total} , $FE_{H_2O_2}$, and $J_{H_2O_2}$. We set aside about 10% of the data set (3 data points) as a test set and used the rest (90% of the data set, 25 data points) as a training set. To avoid potential overfitting, we used 5-fold cross-validation in the training process. Details of cross-validation and training processes are available in the Supporting Information. We first trained SVR models using our initial data set (raw data available in Table S1).¹⁷ In the verification of the prediction, we collected experimental data from 8 additional conditions (raw data available in Table S2) and used the newly obtained data as a new test set for evaluation using the coefficient of determination (R^2) score shown in Figure 3.

Prediction-Based Analysis. We demonstrated prediction-based analysis of the system with thermal efficiency analysis, cost analysis, and production time estimation. We used prediction results of J_{total} , $FE_{\text{H}_2\text{O}_2}$, and $J_{\text{H}_2\text{O}_2}$ and relevant equations for the analysis. Equations and assumptions related to the calculation are available in the Supporting Information.

ASSOCIATED CONTENT

Supporting Information

The Supporting Information is available free of charge at https://pubs.acs.org/doi/10.1021/acsaem.3c00115.

Quantifying H_2O_2 production using UV-vis spectrophotometry; tables of experimental data used in machine learning training; machine learning model training details; thermal efficiency calculation; cost analysis of electrochemical H_2O_2 production calculation; estimated time of H_2O_2 production calculation (PDF)

AUTHOR INFORMATION

Corresponding Author

Xiaolin Zheng — Department of Mechanical Engineering and Department of Energy Science and Engineering, Stanford University, Stanford, California 94305, United States; orcid.org/0000-0002-8889-7873; Email: xlzheng@stanford.edu

Authors

Juyoung Leem – Department of Mechanical Engineering and TomKat Center for Sustainable Energy, Stanford University, Stanford, California 94305, United States; ⊚ orcid.org/ 0000-0002-0690-7784

Lauren Vallez – Department of Mechanical Engineering, Stanford University, Stanford, California 94305, United States; orcid.org/0000-0002-2605-0693

Thomas Mark Gill — Department of Mechanical Engineering, Stanford University, Stanford, California 94305, United States; orcid.org/0000-0002-0108-1012

Complete contact information is available at: https://pubs.acs.org/10.1021/acsaem.3c00115

Author Contributions

J.L. and L.V. contributed equally to this work.

Notes

The authors declare no competing financial interest.

ACKNOWLEDGMENTS

X.L.Z. thanks the National Science Foundation EFRI-DCheM program (Agreement: SUB0000425), Stanford Natural Gas Initiative, and Stanford Woods Institute for the Environment for their generous support. J.L. acknowledges TomKat Center Postdoctoral Fellowship in Sustainable Energy. Part of this work was performed at the Stanford Nano Shared Facilities (SNSF), supported by the National Science Foundation under Award ECCS-2026822.

REFERENCES

- (1) Kampf, G.; Todt, D.; Pfaender, S.; Steinmann, E. Persistence of Coronaviruses on Inanimate Surfaces and Their Inactivation with Biocidal Agents. *J. Hosp. Infect.* **2020**, *104* (3), 246–251.
- (2) Noyori, R.; Aoki, M.; Sato, K. Green Oxidation with Aqueous Hydrogen Peroxide. Chem. Commun. 2003, 3 (16), 1977–1986.
- (3) Targhan, H.; Evans, P.; Bahrami, K. A Review of the Role of Hydrogen Peroxide in Organic Transformations. *J. Ind. Eng. Chem.* **2021**, *104*, 295–332.
- (4) Collivignarelli, M. C.; Abbà, A.; Benigna, I.; Sorlini, S.; Torretta, V. Overview of the Main Disinfection Processes for Wastewater and Drinking Water Treatment Plants. *Sustainability* **2018**, *10* (1), 86.
- (5) Xu, J.; Zheng, X.; Feng, Z.; Lu, Z.; Zhang, Z.; Huang, W.; Li, Y.; Vuckovic, D.; Li, Y.; Dai, S.; Chen, G.; Wang, K.; Wang, H.; Chen, J. K.; Mitch, W.; Cui, Y. Organic Wastewater Treatment by a Single-Atom Catalyst and Electrolytically Produced H₂O₂. *Nat. Sustain.* **2021**, *4* (3), 233–241.
- (6) Guo, Y.; Dundas, C. M.; Zhou, X.; Johnston, K. P.; Yu, G. Molecular Engineering of Hydrogels for Rapid Water Disinfection and Sustainable Solar Vapor Generation. *Adv. Mater.* **2021**, *33* (35), 2102994.
- (7) AL-Omiri, M. K.; Al Nazeh, A. A.; Kielbassa, A. M.; Lynch, E. Randomized Controlled Clinical Trial on Bleaching Sensitivity and Whitening Efficacy of Hydrogen Peroxide versus Combinations of Hydrogen Peroxide and Ozone. *Sci. Rep.* **2018**, *8*, 2407.
- (8) Isaza Ferro, E.; Ruuttunen, K.; Perrin, J.; Vuorinen, T. Sustainable Bleaching of *Eucalyptus Sp.* Kraft Pulp with Hypochlorous Acid, Ozone and Hydrogen Peroxide. *Ind. Crops Prod.* **2021**, *172*, No. 114004.
- (9) Ciriminna, R.; Albanese, L.; Meneguzzo, F.; Pagliaro, M. Hydrogen Peroxide: A Key Chemical for Today's Sustainable Development. *ChemSusChem* **2016**, 9 (24), 3374–3381.
- (10) Yamada, Y.; Fukunishi, Y.; Yamazaki, S.; Fukuzumi, S. Hydrogen Peroxide as Sustainable Fuel: Electrocatalysts for Production with a Solar Cell and Decomposition with a Fuel Cell. Chem. Commun. 2010, 46 (39), 7334–7336.
- (11) Campos-Martin, J. M.; Blanco-Brieva, G.; Fierro, J. L. G. Hydrogen Peroxide Synthesis: An Outlook beyond the Anthraquinone Process. *Angew. Chemie Int. Ed.* **2006**, 45 (42), 6962–6984.
- (12) Shi, X.; Siahrostami, S.; Li, G.-L.; Zhang, Y.; Chakthranont, P.; Studt, F.; Jaramillo, T. F.; Zheng, X.; Nørskov, J. K. Understanding Activity Trends in Electrochemical Water Oxidation to Form Hydrogen Peroxide. *Nat. Commun.* **2017**, *8*, 701.
- (13) Shi, X.; Back, S.; Gill, T. M.; Siahrostami, S.; Zheng, X. Electrochemical Synthesis of H_2O_2 by Two-Electron Water Oxidation Reaction. *Chem.* **2021**, 7 (1), 38–63.
- (14) Fuku, K.; Sayama, K. Efficient Oxidative Hydrogen Peroxide Production and Accumulation in Photoelectrochemical Water Splitting Using a Tungsten Trioxide/Bismuth Vanadate Photoanode. *Chem. Commun.* **2016**, *52*, 5406–5409.
- (15) Liu, J.; Zou, Y.; Jin, B.; Zhang, K.; Park, J. H. Hydrogen Peroxide Production from Solar Water Oxidation. *ACS Energy Lett.* **2019**, *4* (12), 3018–3027.
- (16) Gill, T. M.; Vallez, L.; Zheng, X. The Role of Bicarbonate-Based Electrolytes in H₂O₂ Production through Two-Electron Water Oxidation. ACS Energy Lett. **2021**, 6 (8), 2854–2862.

- (17) Gill, T. M.; Vallez, L.; Zheng, X. Enhancing Electrochemical Water Oxidation toward H2O2 via Carbonaceous Electrolyte Engineering. ACS Appl. Energy Mater. 2021, 4, 12429.
- (18) Mistry, A.; Franco, A. A.; Cooper, S. J.; Roberts, S. A.; Viswanathan, V. How Machine Learning Will Revolutionize Electrochemical Sciences. ACS Energy Lett. 2021, 6 (4), 1422–1431.
- (19) Gill, T. M.; Zheng, X. Comparing Methods for Quantifying Electrochemically Accumulated H₂O₂. Chem. Mater. 2020, 32 (15),
- (20) Pedregosa, F.; Varoquaux, G.; Gramfort, A.; Michel, V.; Thirion, B.; Grisel, O.; Blondel, M.; Prettenhofer, P.; Weiss, R.; Dubourg, V.; Vanderplas, J.; Passos, A.; Cournapeau, D.; Brucher, M.; Perrot, M.; Duchesnay, E. Scikit-Learn: Machine Learning in Python. J. Mach. Learn. Res. 2011, 12 (85), 2825-2830.
- (21) Li, L.; Hu, Z.; Yu, J. C. On-Demand Synthesis of H₂O₂ by Water Oxidation for Sustainable Resource Production and Organic Pollutant Degradation. Angew. Chemie Int. Ed. 2020, 59 (46), 20538-20544.
- (22) Mavrikis, S.; Goltz, M.; Perry, S. C.; Bogdan, F.; Leung, P. K.; Rosiwal, S.; Wang, L.; Ponce de León, C. Effective Hydrogen Peroxide Production from Electrochemical Water Oxidation. ACS Energy Lett. 2021, 6 (7), 2369-2377.
- (23) Patra, S. G.; Mizrahi, A.; Meyerstein, D. The Role of Carbonate in Catalytic Oxidations. Acc. Chem. Res. 2020, 53 (10), 2189-2200.
- (24) Park, S. Y.; Abroshan, H.; Shi, X.; Jung, H. S.; Siahrostami, S.; Zheng, X. CaSnO3: An Electrocatalyst for Two-Electron Water Oxidation Reaction to Form H₂O₂. ACS Energy Lett. 2019, 4 (1),
- (25) Kelly, S. R.; Shi, X.; Back, S.; Vallez, K.; Park, S. Y.; Siahrostami, S.; Zheng, X.; Nørskov, J. K. ZnO As an Active and Selective Catalyst for Electrochemical Water Oxidation to Hydrogen Peroxide. ACS Catal. 2019, 9 (5), 4593-4599.
- (26) Xia, C.; Back, S.; Ringe, S.; Jiang, K.; Chen, F.; Sun, X.; Siahrostami, S.; Chan, K.; Wang, H. Confined Local Oxygen Gas Promotes Electrochemical Water Oxidation to Hydrogen Peroxide. Nat. Catal. 2020, 3, 125-134.
- (27) Mei, B.; Mul, G.; Seger, B. Beyond Water Splitting: Efficiencies of Photo-Electrochemical Devices Producing Hydrogen and Valuable Oxidation Products. Adv. Sustain. Syst. 2017, 1 (1-2), 1600035.
- (28) Wenderich, K.; Kwak, W.; Grimm, A.; Kramer, G. J.; Mul, G.; Mei, B. Industrial Feasibility of Anodic Hydrogen Peroxide Production through Photoelectrochemical Water Splitting: A Techno-Economic Analysis. Sustain. Energy Fuels 2020, 4 (6), 3143-3156.

□ Recommended by ACS

Paired Electrosynthesis of H₂ and Acetic Acid at A/cm² **Current Densities**

Cong Tian, Edward H. Sargent, et al.

SEPTEMBER 11 2023

ACS ENERGY LETTERS

READ 2

Effective Hydrogen Production from Alkaline and Natural Seawater using WO_{3-x}@CdS_{1-x} Nanocomposite-Based **Electrocatalysts**

Mohamed Jaffer Sadiq Mohamed, Anurag Roy, et al.

SEPTEMBER 11, 2023

ACS OMEGA

READ **C**

Thermodynamic and Kinetic Investigation on **Electrogeneration of Hydroxyl Radicals for Water Purification**

Guoshuai Liu, Shijie You, et al

IANUARY 25 2023

ACS ES&T ENGINEERING

READ C

Efficient Voltage-Driven Oxidation of Water and Alcohols by an Organic Molecular Catalyst Directly Attached to a **Carbon Electrode**

Koushik Barman, Michael V. Mirkin, et al.

MARCH 02, 2023

JOURNAL OF THE AMERICAN CHEMICAL SOCIETY

RFAD 🗹

Get More Suggestions >